Physics – Uspekhi **38** (2) 215 – 228 (1995)

PACS numbers: 01.10.Fv

Scientific Session of the Division of General Physics and Astronomy of the Russian Academy of Sciences (26 October 1994)

On 26 October 1994, a scientific session of the Division of General Physics and Astronomy of the Russian Academy of Sciences was held in the P L Kapitza Institute of Physical Problems. The following papers were presented:

(1) **Zh I Alferov, D Bimberg, A Yu Egorov, A E Zhukov, P S Kop'ev, N N Ledentsov, S S Ruvimov, V M Ustinov, I Kheidenraikh** "Strained-submonolayer and quantum-dot superstructures";

(2) **A A Gorbatsevich, V V Kapaev, Yu V Kopaev** "Nondissipative dynamics of electrons in nanostructures";

(3) **A A Bykov, Z D Kvon, E B Ol'shanskii, A L Aseev, M R Baklanov, L V Litvin, Yu V Nastaushev, V G Mansurov, V P Migal', S P Moshchenko** "Quasiballistic quantum interferometer";

(4) **V D Kulakovskii, L V Butov** "Magnetooptics of quantum wires and quantum dots in semiconducting heterostructures";

(5) **V T Petrashov** "New phenomena in metallic mesostructures";

(6) **N S Maslova, Yu N Moiseev, V I Panov, S V Savinov** "Effects of localised states and interparticle interactions on the STM/STS and ASM nanostructure diagnostics".

Below brief summaries of the talks are given.

PACS numbers: 73.90.+f

Strained-submonolayer and quantum-dot superstructures

Zh I Alferov, D Bimberg, A Yu Egorov, A E Zhukov, P S Kop'ev, N N Ledentsov, S S Ruvimov, V M Ustinov, I Kheidenraikh

The self-organisation effects involved in the growth of semiconducting heterostructures, and their use in the fabrication of quasi-one-dimensional and quasi-zero-dimensional structures, have been receiving increasing attention in recent years.

In the present work a new method of fabricating strained InAs/GaAs heterostructures is reported, consisting of successively depositing InAs and GaAs submonolayers on a (110)- or (311)-oriented GaAs substrate ('submonolayer epitaxy'). It is shown that the proposed method improves substantially the optical properties of strained InAs/GaAs heterostructures.

Uspekhi Fizicheskikh Nauk **165** (2) 224 – 238 (1995)
Translated by E G Strel'chenko; edited by H Milligan

The structures were grown with the use of the molecular beam epitaxy apparatus EP-1203. When differently oriented substrates were used, they were placed one next to another on the same mount. The structures intended for photoluminescence and transmission electron microscopy studies were grown on semi-insulating GaAs substrates and consisted of a 140 – 4000 Å GaAs layer which was bounded by a short-period GaAs/AlAs superlattice to prevent nonequilibrium carriers from escaping into the substrate or onto the surface.

In the middle of the GaAs layer, submonolayer InAs/GaAs sublattices or GaAs layers were placed. The InAs part of the structure was grown at a lower temperature (250 – 490 °C) and at increased As beam intensity; the rest of the structure was grown at 600 °C.

Photoluminescent InAs submonolayer structures exhibited an intense and narrow peak in their spectra (less than 1 meV at 5 K), whose long-wavelength shift was governed by the amount of coating applied.

The luminescence excitation spectra for the peak showed very distinctive lines corresponding to excitonic heavy-hole and light-hole resonances. The heavy-hole exciton peaks showed no Stokes shift in their photoluminescence and luminescence excitation spectra.

Samples covered with an InAs submonolayer exhibited anisotropy in both their photoluminescence and luminescence excitation spectra. Linear polarisation in the (011) direction reached 20%.

The results obtained imply a uniform but anisotropic distribution of InAs molecules on a submonolayer-coated GaAs surface and are qualitatively consistent with the formation of oriented chains of InAs molecules.

The luminescent studies of 120 Å quantum well structures based on the $In_xGa_{1-x}As$ solid solution were performed for the same average composition ($x = 0.17$) for (1) usual solid solution, (2) a monolayer (ML) superlattice consisting of 1 ML InAs/5 ML GaAs, and (3) a submonolayer 1 Å InAs/5 Å GaAs superlattice, and showed the submonolayer superlattice to be superior both in terms of luminescence efficiency and emission line width.

Experiments involving long (up to 1000 s) growth interruptions showed that even a monolayer InAs deposit, i.e. one having a far-from-critical thickness, is not stable and transforms into 2 – 3 monolayer thick InAs clusters, with the rest of the surface being coated in a submonolayer fashion. Submonolayer coating remains stable under long growth interruptions. These results explain the superior luminescence properties of submonolayer-epitaxy-grown structures.

With the use of the strain-related mechanism, quantum-dot GaAs-matrix structures were fabricated both with

submonolayer epitaxy-grown solid solutions and with deposition of pure InAs. The monitoring of the process led to the conclusion that in the InAs/GaAs case the critical thicknesses depend on the In/Ga ratio and that the formation process itself may be slowed down considerably by reducing the growth temperature.

Direct transmission electron microscopy showed that, both in growing a submonolayer 1 Å InAs/1 Å GaAs superlattice and in depositing pure InAs of equivalent 12–14 Å average thickness fairly ordered systems of pyramidal quantum dots form. The dots are about 120–140 Å in height and their bases are [010]- or [001]-oriented squares of 30 Å side.

The atomically resolved cross-sectional image of the quantum dots showed the (320) faces to be monatomically smooth. It was also found that a planar GaAs surface is restored on growing over the dots a 50 – 70 Å layer.

Photoluminescent quantum dot structures displayed an intense luminescence line strongly shifted toward longer wavelengths from the expected location of the uniform well. The maximum wavelength (1.2 μm) was obtained for the structure with an average InAs layer thickness of 12 Å.

Upon a local electron-beam excitation, the smooth luminescence line, with a halfwidth of about 2.0 meV (for 5 K), became a series of supernarrow (about 0.1 meV) luminescence lines, each of which originated from its respective individual quantum dot and retained its halfwidth as the temperature was increased. This is direct spectroscopic evidence for the delta-like behaviour of the density of states in quantum dots.

The luminescence efficiency of quantum dot structures was at all temperatures ($1.6\ \mathrm{K} < T < 300\ \mathrm{K}$) comparable to that of high-quality GaAs/AlAs quantum well structures.

A separate-confinement AlGaAs–GaAs laser structure with varying refractive index in the optical confinement region was grown. The fabrication process involved the introduction of an InGaAs quantum-dot layer into the middle of the 140 Å thick GaAs recombination region.

With the aid of injection excitation at 300 K, laser emission via quantum dot states was obtained for the first time, with a threshold current density below 1 kA cm^{-2} and differential quantum efficiency up to 70%.

In the temperature range 50 – 120 K, a temperature dependence of the threshold current density was observed. The characteristic temperature $T_0 = 350\ \mathrm{K}$ exceeded the theoretical value for quantum well lasers.

PACS numbers: 72.90.+y

Nondissipative dynamics of electrons in nanostructures

A A Gorbatsevich, V V Kapaev, Yu V Kopaev

Recently [1, 2], a new data transmission–data processing method has been proposed, based on controlled redislocation of electron wave functions $\psi(r, t)$ in nanostructures. Such redislocation corresponds directly to the desired data transformation mode. The data carrier is here the integral probability $|\psi(r)|^2$ in some region of the nanostructure.

1. Redislocation may be achieved by electric voltage, when to different voltage values there correspond different stationary electronic states with the required distributions $|\psi(r)|^2$. A change from one distribution to another (a redislocation) in accord with a prescribed law $\psi(r, t)$ can be achieved by adiabatic application of a voltage $U(t)$, whose time dependence may be determined by employing the adiabatic-quasiclassical analogy proposed by Landau [3]. This method is valid only for slow redislocations.

In the opposite extreme, when the voltage corresponding to a new stationary state, with a required distribution $|\psi(r)|^2$, is switched on in a step fashion, quantum beats appear in accordance with the time-dependent Schrodinger equation.

The new stationary (free-of-beats) state is only established via dissipative processes. As a result, redislocation is a rather slow process involving dissipation of electric power and heat release. It then becomes impossible to implement the necessary time dependence of redislocation.

Is it possible to make the switching fast (anti-adiabatic) and nondissipative?

The present work shows that the aforementioned analogy between the temporal and spatial problems, established by Landau [3] for the adiabatic regime, is amenable to extension: when one needs to consider only two electronic levels, the temporal problem reduces to a static spatial scattering problem, where the time-dependent electric voltage is related to a potential which is a function of the spatial coordinates.

As regards the latter, it is known that nonreflecting potentials exist. An example is resonance tunnelling. Thus, for a given nanostructure a variation of voltage with time can be found for which quantum beats are absent, i. e. the transition induced by a voltage with a prescribed time dependence will correspond to a monotonic transition from one stationary state (with no voltage) to another (with voltage present).

It is shown that a nonreflecting state (no quantum beats) can be approximately reached for a two-level model by switching on the voltage in two steps. The voltage applied in the first step must then correspond to the resonance tunnelling condition, with the duration of the step equal to the half-period of the quantum beat at resonance. During this time a complete redislocation occurs as a result of resonance tunnelling. If the voltage is at this moment abruptly increased, with inversion of the electronic levels relative to the original state, the amplitude of the quantum beats will become smaller as one moves away from the resonance.

A three-level model requires that voltage be switched on in three steps, the first step corresponding to the resonance between the first and the second levels, and the second to the resonance between the second and the third levels. As before, the third step is needed to move the levels out of resonance, thus ensuring that the beats are small.

What is important for practical application is that approximately the same type of electron evolution can be obtained for a voltage increasing monotonically (say, linearly) in time, by appropriately choosing the slope and the duration.

For a three-well system, a switching regime can be found for which the electron concentrations in the end wells differ considerably at each instant of time. Such behaviour proves to be important for devising a quantum analogue to a system of complementary field transistors [1, 2].

2. We have also considered an alternative way of controlling electron redislocation, which involves an elec-

tromagnetic field with a frequency corresponding to the separation between electronic levels. Since nanostructure dimensions are typically of the order of 10^{-6} cm, and the level separations are of the order of 10^{-2} eV, fields $E \sim 10^3 - 10^4$ V cm^{-1} can be regarded as strong. The effect of the field on the electrons is conveniently described by the method of Floquet functions combined with the quasi-energy representation.

We have introduced a temporal analogy of the Kronig–Penney model, with the dependence $E(t) = E_0 \cos \omega t$ replaced by a time-periodic sequence of rectangular pulses. In the two-level case, the model enables many results to be obtained analytically. For a multiwell system, numerical simulation is considerably simplified compared to the $E(t) = E_0 \cos \omega t$ case.

A convenient concept to introduce is the Brillouin zone, not in momentum space as for spatially periodic potentials, but rather in energy space. The characteristic points in the variation of the quasi-energies with field amplitude E_0 (or field frequency ω) are the anticrossing points (where the quasi-energies are pushed apart when approaching one another) and the crossing points (where they cross). For symmetric systems, an anticrossing point corresponds to a resonance with an odd number of photons (weak field Rabi oscillations), and the crossing points to an even number.

If the electronic and field parameters are those corresponding to the crossing points, the tunnelling between the quantum wells is effectively suppressed (redislocation suppression). For the anticrossing points, the reverse situation obtains.

In the weak field case, a (multiphoton) odd-photon resonance corresponds to oscillations with the probability amplitude unity (Rabi oscillations) for interlevel transitions. The oscillation frequency depends on the field intensity and turns out to be much less than the field frequency. Level population oscillations correspond to the periodic redislocation between the wells.

Increasing field intensity increases the frequency of the Rabi oscillations, and in strong fields oscillations arise whose amplitude is unity at the field frequency and is appreciable at multiples of ω. Since a multiple frequency gives rise to electron redislocation, it also causes a change in polarisation, with a dipole moment proportional to the size of the nanostructure (about 10^{-6} cm). For this reason, a massive generation of higher harmonics is to be expected.

Note that such generation occurs in the case of a weak field, when the system of asymmetric quantum wells has its levels equidistant and it is through these levels that multiphoton absorption takes place [4]. For strong-field multiphoton resonance, such equidistant levels are in effect induced by the field, since the quantity to be given a direct physical meaning is quasi-energy, defined to within an arbitrary number of photon energies $\hbar\omega$ (by analogy with umklapp processes).

The problem of level-to-level transitions and associated field-induced redislocation in a two-well system is analogous to that of multiphoton atom ionisation. In the latter case we have a transition from the ground state to continuous spectrum and, on ionisation, electron escape to infinity. Since the multiphoton ionisation probability is appreciable only if the field is sufficiently large, ionisation by tunnelling becomes important.

The work of Keldysh [5] has demonstrated that, if the field amplitude–frequency relation is such that the field period is larger than the tunnelling time through the barrier (where the barrier is due to the Coulomb potential and the wave electric field of the wave), then the dominant ionisation mechanism is by tunnelling. For our problem (interwell electron redislocation), of practical importance is a redislocation probability of order unity, i. e., one implying the proximity of an anticrossing point.

For a symmetric quantum well system, to the anticrossings lying in the (ω, E_0) (frequency – amplitude) plane there corresponds a set of continuous curves characterised by the number of photons involved in the resonance. The field frequency along the curves increases monotonically with amplitude, owing to the monotonic (and field sign symmetric) increase in the level separation. As a result, the multiphoton contribution to the redislocation predominates over the tunnelling one, because for a symmetrical system the resonance tunnelling condition is met in the absence of the field, and increasing the field moves the system away from the resonance.

In contrast, for a nonsymmetric system resonance tunnelling occurs at finite E_r and only for one particular sign of the field. In the other half-wave, the system moves away from the resonance tunnelling condition.

An important feature in this context is the difference in electron level separations between the positive and negative field half-waves. As a consequence, the anticrossing multiphoton resonance occurs only for a discrete set of points in the frequency–amplitude plane for which the ratio of level separations in the positive and negative half-waves corresponds to a ratio of integers.

Note that photon resonances in the positive and negative half-waves correspond to different numbers of photons. In the (ω, E_0) plane there exists a region near E_r in which the set of anticrossing points corresponds to minima (in frequency) characterised by the number of resonance photons for either half-wave. In this region, resonance tunnelling dominates redislocation.

A similar discrete set of points exists in the (ω, E_0) plane for the quasi-energy crossing (i.e. redislocation suppression) condition.

The dramatic change in redislocation probability on field amplitude or frequency change in the transition from crossing to anticrossing may be used in optoelectronic components for the purpose of converting an electromagnetic signal to an electric one.

It is expected that the above features of the interaction of the electromagnetic field with electrons in quantum wells may prove to be of relevance to the operation of intersubband transition lasers.

References

1. Gorbatsevich A A, Kapaev V V, Kopaev Yu V, Kremlev V Ya *Physics of Low-dimensional Structures* **4/5** 57 (1994)
2. Gorbatsevich A A, Kapaev V V, Kopaev Yu V, Kremlev V Ya *Mikroelektronika* **23** 17 (1994)
3. Landau L D, Lifshitz I M *Kvantovaya Mekhanika* (Moscow: Nauka, 1974) § 53 [*Quantum Mechanics* (Oxford: Pergamon Press, 1981)]
4. Rosencher E, Bois P H *Phys. Rev. B* **44** 11315 (1991)
5. Keldysh L V *Zh. Exp. Teor. Fiz.* **47** 1945 (1964) [*Sov. Phys. JETP* **20** 1307 (1965)]

PACS number: 07.60.Ly

Quasiballistic quantum interferometer

A A Bykov, Z D Kvon, E B Ol'shanskii, A L Aseev, M R Baklanov, L V Litvin, Yu V Nastaushev, V G Mansurov, V P Migal', S P Moshchenko

Since the communication by Webb et al. [1], ring-shaped electron interferometers have been studied for several years now, particularly after the observation of Aharonov–Bohm oscillations in the quasiballistic regime, with a mean free path $l > L$ (where $L = \pi d_{\text{eff}}/2$) [2, 3].

This interest stems primarily from the fact that the electron interferometer lies at the heart of the quantum interference transistor, which promises orders-of-magnitude switch power reduction compared to classical transistors. The development of the interference transistor has already run into difficulties, owing primarily to the suppression of interference effects by the fluctuating potential of impurities and defects [4]. One way to resolve this is to reduce the size of the device.

In what follows we report on the fabrication and properties of a quasiballistic electron interferometer with an effective ring diameter $d_{\text{eff}} = 600-700$ nm and conducting channel width $W < 20$ nm. The authors are not aware of any descriptions of an interferometer that small. Because of the size of the device it proved possible, for the first time, to achieve a single-mode interferometer operation and to observe the interference of boundary current states.

The interferometer was fabricated by electron beam lithography and reactive ion etching on the basis of a $2D$ electron gas in an AlGaAs/GaAs heterojunction grown by molecular beam epitaxy with a thin spacer layer. The electron gas parameters at $T = 4.2$ K were as follows: surface electron density $N_S = (7-9) \times 10^{11}$ cm^{-2} and the mobility $\mu = 10^5$ cm^2 V^{-1} s^{-1}. This corresponds to an electron mean free path $l = 1.5$ μm.

We emphasise that it is the use of a heterojunction with a thin (3 nm) spacer layer and hence with a high density of $2D$ electrons which enabled an interferometer with a very narrow conducting channel ($W < 20$ nm) to be developed.

Electron lithography was conducted in a raster electron microscope (Stereoscan S-2A) with the use of the image generator ELPHY-1. The interferometer was formed on a Hall mesostructure obtained by standard photolithography. The bridge width and the potentiometer contact separation were 10 and 100 μm, respectively. The interferometer ring was fabricated by exposing a circle of 400 nm diameter with a circular space 200 nm wide, framed by 200 nm wide lines.

The electron-resist image development was followed by reactive ion etching of GaAs and AlGaAs conducted so as to finish the etching process in AlGaAs. The raster electron micrograph of the interferometer is given in Fig. 1. Fig. 2 shows a schematic cross-sectional diagram of the device and indicates its basic dimensions.

The interferometer magnetoresistance was measured at temperatures $T = 0.02-4.2$ K in magnetic fields up to 10 T. Resistance measurements were made on an alternating 30 Hz signal with a four-probe scheme using a phase detector.

Fig. 3 presents the results of these measurements as a function of magnetic field for $T < 0.1$ K. In the figure one sees Aharonov–Bohm oscillations, whose amplitude is

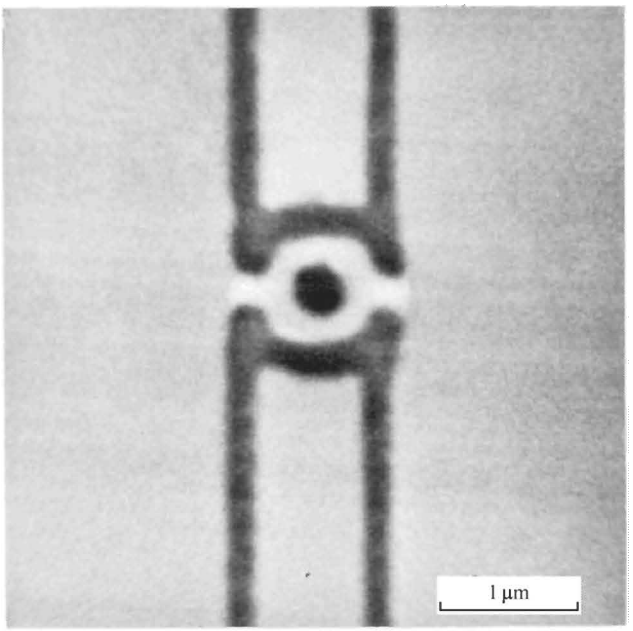

Figure 1. Scanning electron micrograph of the interferometer (×27 500).

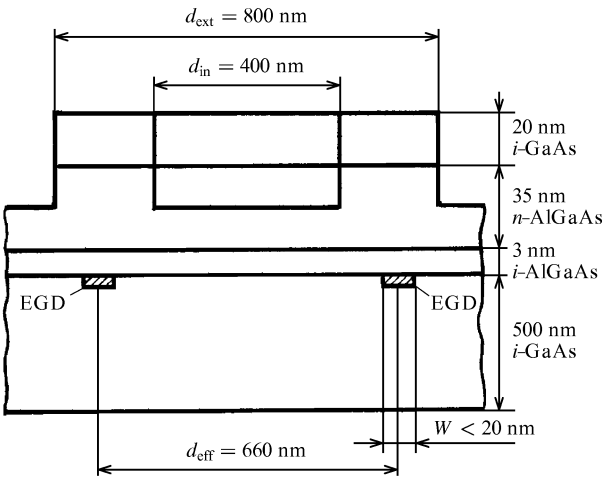

Figure 2. Cross section of the ring structure, with basic dimensions.

comparable with the total sample resistance, and whose period in magnetic field is $\Delta B = 0.0115$ T, which corresponds to the quantisation of a magnetic quantum flux $\Phi = h/e$ through an area with effective diameter $d_{\text{eff}} = 660$ nm (h/e oscillations).

Another feature apparent in Fig. 3 is that the oscillation amplitude depends strongly on the magnetic field. At $B = 0.75$ T it was a maximum when $\Delta R/R_0 = 0.35$ [5]. To date, the maximum amplitude seen was in the experiments of Refs [3, 6], with $\Delta R/R_o = 0.2$. In addition to the fundamental oscillation there are also beats, whose period is 10 times the fundamental one. The fundamental amplitude is strongly reduced the instant the beats set in (virtually down to zero for certain fields).

The beats are apparently due to the finite width, W, of the interferometer conducting channels. Knowledge of the beat period allows one to estimate the width W from the relation $4W/d = \Delta B/B_{\text{b}}$ (where B_{b} is the beat period). The result is $W = 15-20$ nm. An estimate shows that at such

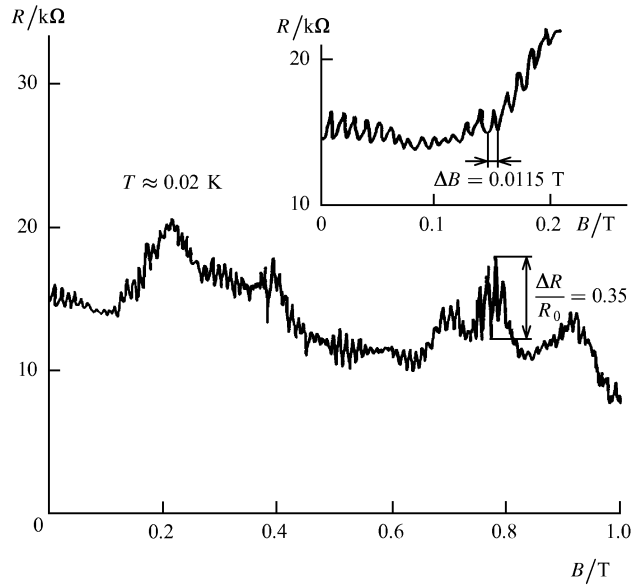

Figure 3. Interferometer resistance plotted against magnetic field for $T < 0.1$ K (inset: Aharonov – Bohm oscillations close to the beat minimum).

values of W only the fundamental one-dimensional subband is filled. This estimate is supported by the exact numerical calculations, carried out by Tkachenko and coworkers, of the electron energy spectrum and of the form of the electron-wave-carrying well.

Thus we can conclude that our device attains the single-mode electron waveguide regime. It is for this reason that the present work yields large Aharonov–Bohm amplitudes even though the two-dimensional electrons are much less mobile when compared to the data of Refs [3, 6].

The above data also support the interesting theoretical prediction [7] that Aharonov–Bohm oscillations in a one-dimensional ring interferometer may be large even if electron scattering is strong.

Together with the h/e oscillations described above, $h/2e$ Aharonov–Bohm oscillations were observed. These latter are an order-of-magnitude smaller in amplitude and appear as either inflections or additional minima in the regions dominated by the fundamental oscillations. They may dominate, however, at the instant when beats occur (see the inset in Fig. 3).

It should be noted that the $h/2e$ oscillations in this case are unrelated to the weak localisation effects, because these oscillations exist in magnetic fields which prevent weakly localised $h/2e$ oscillations [8]. We believe that they are due to the interference of two independent back-scattering trajectories. A similar picture was observed by Ford et al. [3].

Owing to the narrow conducting channels of the device, it has proved possible for the first time to observe effects due to the interference of edge current states and to resonance tunnelling between them. These effects are manifested as magnetoresistance oscillations, which differ in frequency and appear in the strong magnetic fields corresponding to the incipient quantum Hall effect regime [9].

The occurrence of these effects is also greatly influenced by random-impurity potential fluctuations, which may render the conducting channels nonuniform in width. The result is that while in some regions of the interferometer the edge states are well separated, in others channel narrowing causes a substantial increase in the wave function overlap between opposite edge states. This enables the electrons to move from one edge to the other as a result of tunnelling operating simultaneously with potential fluctuation scattering.

References

1. Webb R A et al. *Phys. Rev. Lett.* **54** 2696 (1985)
2. Timp G et al. *Phys. Rev. Lett.* **58** 2814 (1987)
3. Ford C F D et al. *Appl. Phys. Lett.* **54** 21 (1989)
4. Fowler A B *Granular Nanoelectronics* (NATO ASI Series, Physics B, Vol. 251) (New York: Plenum Press, 1991)
5. Bykov A A et al. *Pis'ma Zh. Exp. Teor. Fiz.* **57** 596 (1993) [*JETP Lett.* (1993)]
6. Ismail K, Washburn S, Lee K Y *Appl. Phys. Lett.* **59** 1998 (1991)
7. Gefen Y, Imry J, Azbel M Ya *Phys. Rev. Lett.* **52** 129 (1984)
8. Al'tshuler B L, Aronov A G, Spivak B Z *Pis'ma Zh. Exp. Teor. Fiz.* **33** 101 (1993) [*JETP Lett.* (1993)]
9. Bykov A A et al. *Pis'ma Zh. Exp. Teor. Fiz.* **58** 897 (1993) [*JETP Lett.* (1993)]

PACS numbers: 73.61.Jc; 78.20.Ls

Magnetooptics of quantum wires and quantum dots in semiconducting heterostructures

V D Kulakovskii, L V Butov

Artificial electronic systems with small dimensions are of considerable interest both for fundamental reasons and from the point of view both of theory and of device application. The unidirectional quantisation of electronic motion is easily achieved in semiconducting heterojunctions grown by molecular beam epitaxy. Studies of quasi-two-dimensional (2D) electronic systems in quantum wells (QW) with high quality interfaces have revealed a range of novel phenomena in both their transport and optical properties.

Further major changes in properties are expected to occur when the dimensions of the system in the QW plane are reduced to the nanometer scale. The most common method for obtaining 1D and 2D quasi-systems (quantum wires and quantum dots) is high-resolution electron beam lithography followed by etching of the QW layer.

An indication of the quantisation of the in-plane electronic motion is usually the shift upwards in exciton energy. However the shift may be of some other origin, such as additional strains in the system, etc.

Sufficiently reliable data on QW-plane quantisation may be obtained by measuring transition energies between the excited subbands that result from the dimensional quantisation of the in-plane motion of the carriers. This is most conveniently done on InGaAs/GaAs wells, which have simple conduction bands and a simple valence band (owing to the large strains in the InGaAs layer caused by the difference in lattice parameters between InGaAs and GaAs).

The QW heterojunctions for fabricating quantum wires and quantum dots were grown by molecular beam epitaxy on the (100) surface of undoped GaAs. The structures

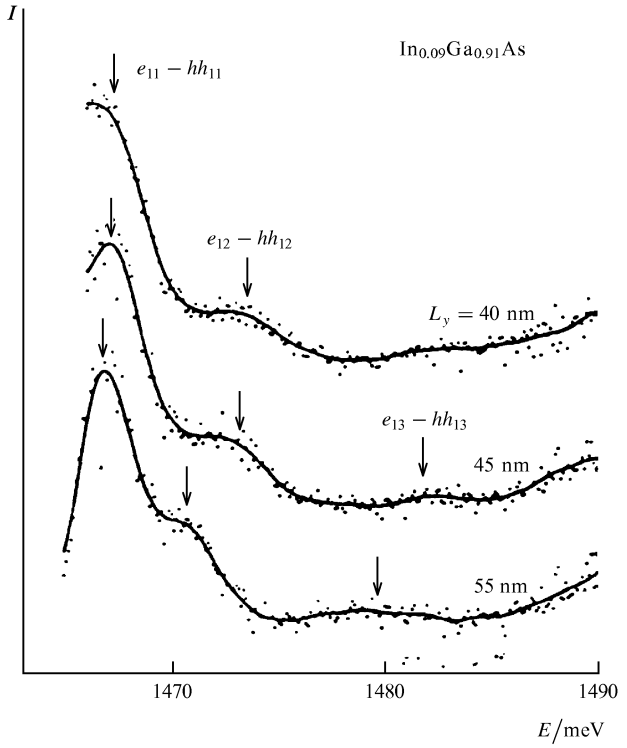

Figure 1. Exciton emission photoexcitation spectra for a quantum wire with $L_y = 40-50$ nm.

consisted of a 500 nm GaAs buffer, 4.9 nm InGaAs well with 9 to 20% In content, and a 15 nm GaAs layer on the InGaAs surface. The fabrication method employed high-resolution electron beam lithography, Al masking, and selective chemical etching. The etching agent removes the surface GaAs layer between the Al masks, thus causing potential modulation in the QW plane.

As a first approximation, the regions can be considered as GaAs/InGaAs/GaAs and vacuum/InGaAs/GaAs. The dimension of the quantum wires and quantum dots in the QW plane was varied from a few hundred nm to 25 nm. The width of a quantum wire was determined by the use of a scanning electron microscope.

Quantum-wire emission spectra at low excitation densities are dominated by the exciton emission line. For a quantum wire with $L_y > 60$ nm, the line position is virtually independent of L_y. As L_y is decreased further, the transition energy increases due to the in-plane quantisation. The half-width of the emission line remains unchanged as L_y is decreased down to 40 nm. For lower L_y, it increases because of quantum-wire width fluctuations. Estimates show that the fluctuations in L_y are within 7 nm.

The exciton-emission photoexcitation spectra for quantum wires with $L_y = 40-50$ nm are shown in Fig. 1. The long-wavelength peak corresponds to the resonance emission in the exciton ground state $e_{11}-h_{11}$.

Of particular interest, in connection with photoexcitation spectra, are additional spectral features, denoted as $e_{12}-hh_{12}$ and $e_{13}-hh_{13}$, which correspond to the additional quantisation of the in-plane motion of electrons and holes. These peaks are absent from the emission spectrum of the QW used in quantum wire fabrication. As L_y is increased, the peaks are shifted toward higher energies owing to the increased energy of the y axis quantisation.

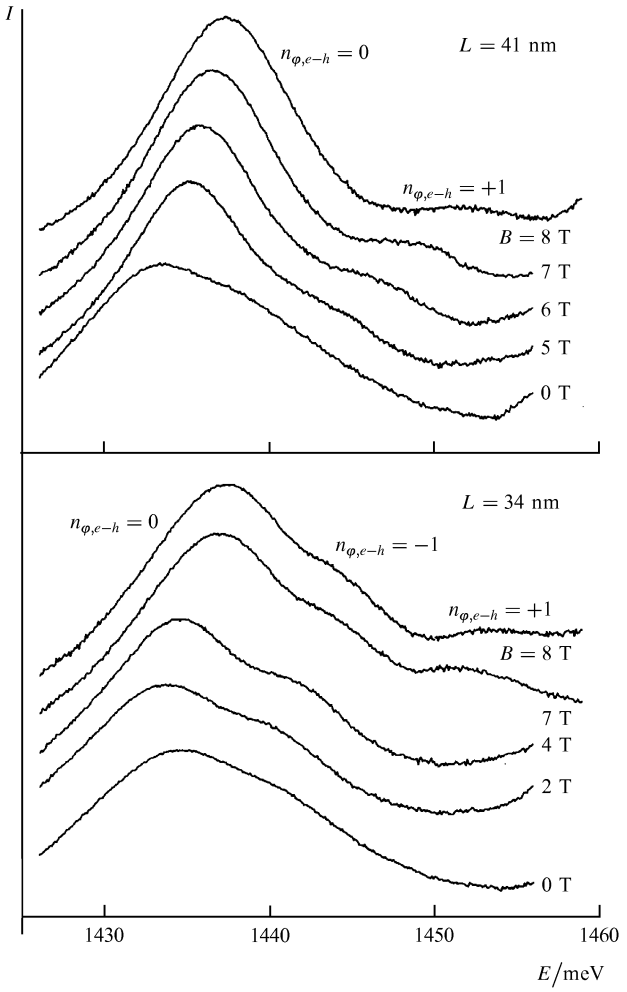

Figure 2. Quantum dot photoluminescence spectra as a function of magnetic field at high excitation density.

Additional peaks, due to the QW-plane quantisation of the electrons and holes, are also seen in the luminescence spectra at excitation densities large enough for the photo-excited carriers to occupy several of the subbands that result from the dimensional in-plane quantisation.

Comparison shows that the transition energy differences $e_{11}-hh_{11}$ and $e_{12}-hh_{12}$ differ considerably in the photo-excitation and photoluminescence spectra. The reduction in the transition energy splitting observed in quantum wires with a high density of photoexcited carriers is due to the electron–electron and electron–hole interactions.

On going from the case of the quantum wire to the quantum dot, the reduced dimensionality causes the transition energy to increase faster with decreasing quantum dot size. A marked increase in the energy of the fundamental transition in the quantum dot can be seen even at $L \approx 70-80$ nm (where L is the quantum dot diameter). To detect higher state emission, higher excitation densities were used. Of particular interest in this case is the behaviour of the transition energies in a magnetic field B normal to the quantum dot plane.

In Fig. 2 the quantum dot photoluminescence spectra are plotted as a function of magnetic field [1]. In zero field one sees the lines $1e-1h$ and $2e-2h$ for the allowed transitions involving states from the first and second

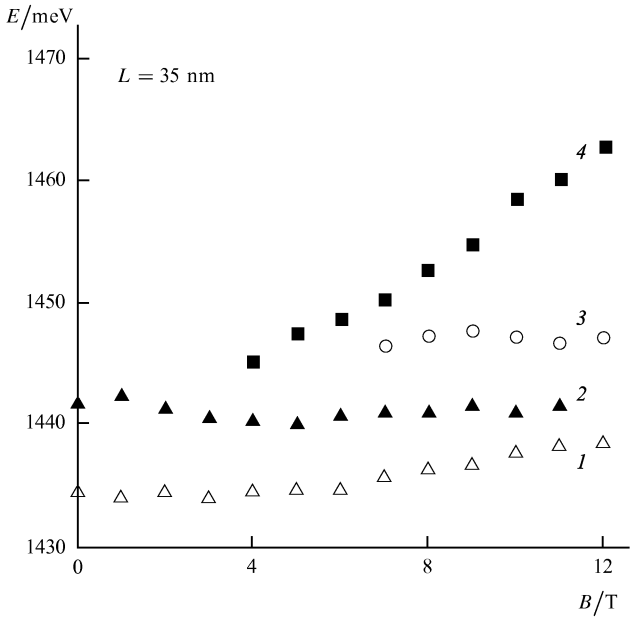

Figure 3. Transition energies in quantum dot photoluminescence spectra versus magnetic field.

dimensional quantisation levels. In a magnetic field, line splitting is observed.

The transition energies as a function of magnetic field are shown in Fig. 3, where they are seen to behave qualitatively differently from the 2D quantum well magnetoexciton states. Thus, in two dimensions the dependence of the energy of optically active 2D magnetoexcitons on B has the shape of an open fan [2]. In a quantum dot, in addition to the diverging lines *1* and *4* characteristic of the quantum well, there are lines *2* and *3*, whose energies increase with magnetic field more slowly than does the energy of the fundamental transition (*1*). The presence of such terms is a specifically quantum dot feature [3, 4].

The appearance of such terms can be qualitatively explained by considering the strong-field limit (magnetic length $L_B \ll L$). In this limit the confinement of excitonic motion to the xy plane, due to the weak quantum dot potential, may be treated as a perturbation. The sequence of lower exciton levels is then determined by the dimensional quantisation of the magnetoexciton centre-of-mass motion in the quantum dot potential.

As a consequence, the state energy splitting ΔE is determined by the magnetoexciton effective mass $M_{ex} = 2\hbar^2/E_0 l_B^2 \sim B^{1/2} \gg m_e + m_h$ (where $E_0 = \frac{1}{2}\sqrt{\pi}e^2/\varepsilon l_B$ is the magnetoexciton binding energy) and decreases with field. Thus, for a parabolic quantum dot [4] the splitting is

$$\Delta E \sim \hbar\left(\frac{m_e\Omega_e^2 + m_h\Omega_h^2}{M_{ex}}\right)^{1/2},$$

where Ω_e and Ω_h are electron and hole frequencies for the parabolic quantum dot potential.

The large linewidths found in the measured emission spectra of the artificial (i.e. fabricated by lithography or etching) quantum dots are due primarily to dot size fluctuations. The study of single-quantum-dot spectra is limited by the rather low quantum yield that current technologies offer for quantum dots in direct contact with a surface.

However, the physics of the quasistate 0D in semiconducting structures can be studied not only on artificial but also on so-called natural quantum dots formed by random potential fluctuations due (for example) to QW width or composition fluctuations.

Convenient natural quantum dots to study are electric-field-tunable AlAs/GaAs coupled wells [5]. Their advantages are the long lifetime of indirect excitons and the possibility of the resonant injection of carriers onto GaAs quantum dot levels.

The heterostructures were grown by molecular beam epitaxy without growth interruptions and took the form of $n^+ - i - n^+$ diodes with a pair of AlAs/GaAs layers between $Al_{0.48}Ga_{0.52}As$ barriers.

The band diagram of the active part of the structure at a negative gate voltage ($-V_g$) is given in the left inset in Fig. 4. The relative energies of the Γ electrons in GaAs and X electrons in AlAs were rearranged by varying V_g thus enabling a $\Gamma - X$ transition. In an indirect regime, the exciton lifetime increased up to $\tau > 100$ ns, much longer than the direct-regime lifetime of $\tau < 1$ ns. The V_g dependences of the photoluminescence energies in the direct $(E_0^\Gamma - HH_0)$ and indirect $(E_0^X - HH_0)$ transitions are shown in the right inset of Fig. 4. The theoretical dependences (neglecting $\Gamma - X$ mixing) are shown as solid lines.

Fig. 4 shows the photoluminescence spectra in the indirect regime for two values of the excitation spot diameter d. In Fig. 4a ($d = 100$ μm) the direct $(E_0^\Gamma - HH_0)$ and indirect $(E_0^X - HH_0)$ transitions are seen. The line shapes are characteristic of nonuniformly broadened photoluminescence lines for quantum wells of uninterruped growth. Decreasing the excitation spot diameter leads to qualitatively new spectral features, the sharp lines 1–7 in Fig. 4b.

In recording narrow-gap spectra, the linewidth is about 0.2 meV. These narrow lines are reminiscent of the photoluminescence spectra of 0D excitons in a single artificial quantum dot [6]. The lowest energy photoluminescence peak is 30 meV below the D line and 38 meV below the direct absorption edge, in approximate correspondence to a two-monolayer fluctuation in the GaAs well width.

Although strictly reproducible for a fixed point on the sample, the photoluminescence spectrum changes considerably when the QW plane is scanned. Whereas the position of the $E_0^X - HH_0$ line is determined by the gate voltage V_g (see the left inset in Fig. 4), the position of the sharp lines is virtually V_g independent. The lack of Stark shift in and the high intensity of the sharp lines detected indicate that they correspond to direct transitions from the 0D states in the local potential minima in the GaAs well.

By studying the manner in which the sharp-line pattern changes with the position of the excitation spot on the sample surface it proved possible to investigate the potential map of the GaAs well. The picture obtained is in agreement with the idea of the well as a disordered array of arbitrarily sized quantum dots. The splitting between the sharp lines contains information about the extent of the potential minimum.

Analysis reveals a large variation of QW width fluctuations in the xy plane. Fluctuations in potential destroy the overlap between the delta-like contributions of different quantum dots to the density of states, and lead to the nonuniform broadening of the latter .

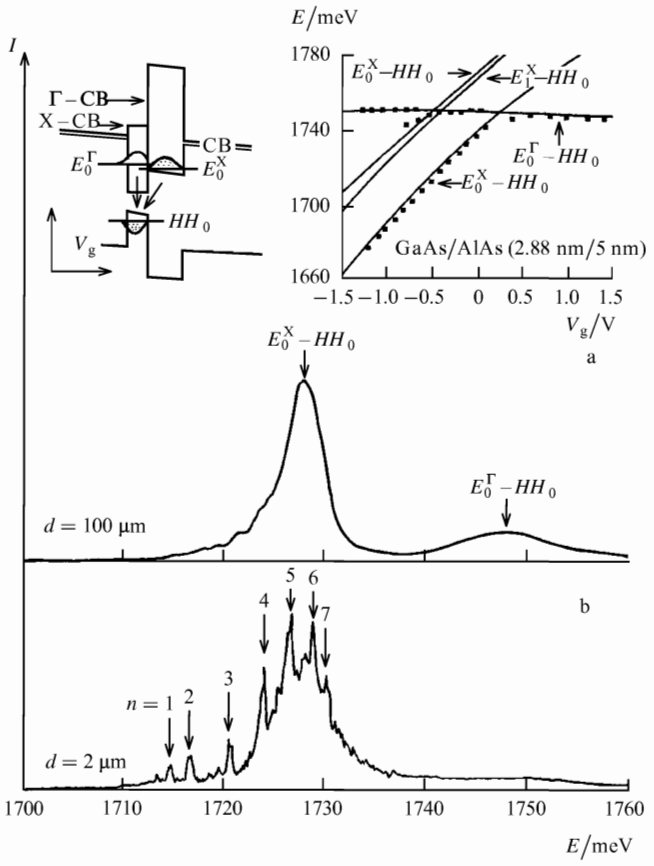

Figure 4. Photoluminescence spectra of GaAs/AlAs coupled QWs (3 nm/5 nm) in the indirect regime ($T = 4.8$ K, $V_g = -0.2$ V): (a) $d = 100$ μm; (b) $d = 2$ μm. Insets: schematic band diagram; the observed transition energies versus gate voltage.

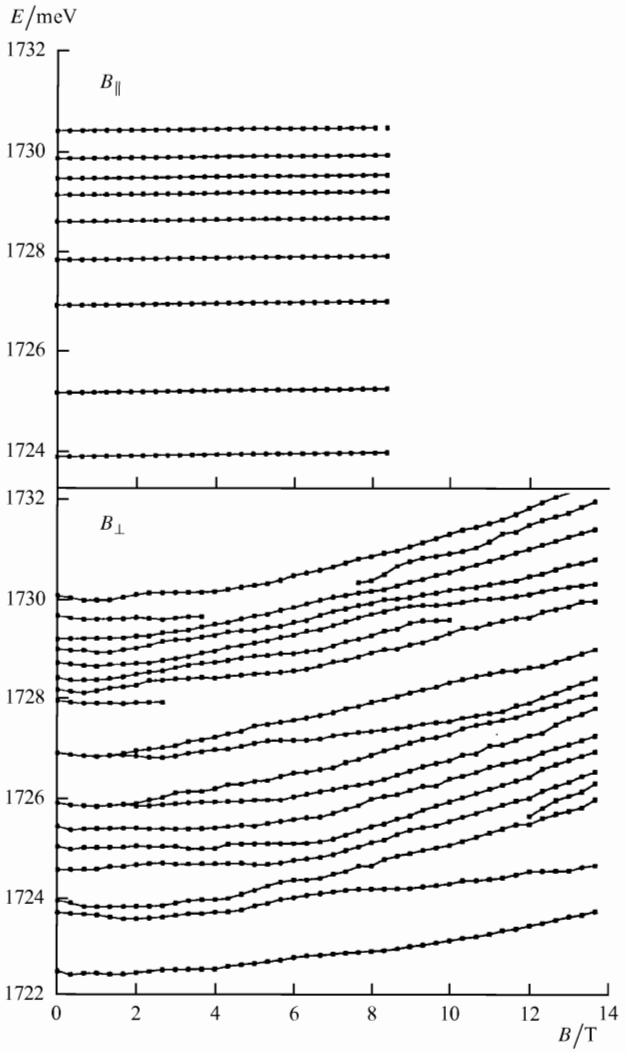

Figure 5. Positions of sharp lines in the emission spectra of natural quantum dots in GaAs/AlAs coupled QWs (3 nm/4 nm) as a function of a magnetic field parallel ($B_\parallel$) and normal ($B_\perp$) to the QW plane ($V_g = 0.1$ V).

Because the natural quantum dots under study are strongly quantised in the z direction and weakly quantised in the xy plane, the response of interband transitions to the magnetic field should be different depending on whether the field is in ($B_\parallel$), or normal to ($B_\perp$) the QW plane. The position of the sharp lines as a function of $B_\perp$ and $B_\parallel$ is shown in Fig. 5. Since changing the direction of the field relative to the QW plane required a replacement of the sample, the data obtained correspond to different quantum dots on the QW surface. The diameter of the excitation spot in our experiment was about 10 μm, so lines from only a few potential minima were present in the spectrum.

In Fig. 5 it is seen that whereas $B_\parallel$ has little or no effect on the position of the sharp lines, marked line shifts, splittings, and anticrossings are observed for $B_\perp$. The complexity of the data is partly due to the fact that contributions from several potential minima are involved. Nevertheless, the dependence of the positions of the lowest four lines (which presumably correspond to one potential minimum) are in qualitative agreement with the theoretically predicted magnetic field dependence of the quantum dot exciton terms [3].

The spectroscopy of semiconducting structures with high spatial resolution enables the exciton properties of natural quantum dots to be investigated. This avoids the labour-intensive fabrication of artificial quantum dots.

Recently, sharp 0D-state photoluminescence lines from single quantum wells have been found [7, 8]. In contrast to their coupled counterparts, for which there is the possibility of resonance injection of long-lived carriers, single QWs require higher spatial resolution for 0D states to be detectable. In Ref. [8] both excitons and biexcitons were examined in natural quantum dots.

The authors are grateful to H Abstreiter, A Vorhel, G Weiman, A Zrenner, M Bayer, A A Dremin, I E Itskevich and A Schmidt for their cooperation, and to V B Timofeev for helpful discussions. The financial support of the Russian Foundation "Nanostructures" and of the Volkswagen Foundation is gratefully acknowledged.

References

1. Bayer M, Reinecke T L, Schmidt A et al., in *Proc. 22th Int. Conf. Semic. Phys., Vancouver, Canada, 1994*
2. Shinada M, Sugano S *J. Phys. Soc. Jpn.* **21** 1936 (1966)
3. Halonen V, Chakraborty T, Pietilainen P *Phys. Rev. B* **45** 5980 (1992)
4. Dzyubenko A B, Sivachenko A Yu, in *Proc. 3th Int. Conf. Opt. Exc. Conf. Syst., Montpellier, France, 1993*
5. Zrenner A, Butov L V, Hagn M et al. *Phys. Rev. Lett.* **72** 3382 (1994)

6. Brunner K et al. *Phys. Rev. Lett.* **69** 3216 (1992)
7. Hess H F, Betzig E, Harris T D et al. *Science* **264** 1740 (1994)
8. Brunner K et al. (to be published)

PACS numbers: 73.40.Vz

New phenomena in metallic mesostructures

V T Petrashov

Introduction. The last few years have seen the appearance of a new area in mesoscopic research, the investigation of 'hybrid' metallic mesoscopic structures made up of materials widely different in their electronic and magnetic properties. Such systems conserve the coherence of electrons in their interlayer motion, and exhibit quantum mechanical mechanisms by means of which the inner and external boundaries affect the electron transport. This is reminiscent of the effects of mirrors in optical interferometers.

Of particular interest are hybrid structures from whose boundaries electrons are reflected in a manner which permits control of their phase shift. Examples are structures consisting of normal (N) and superconducting (S) layers [1–12]. On reflection from an N/S interface the electron phase alters in a deterministic way and the coherence is not violated. A reflected normal electron creates a Cooper pair in the S layer and becomes a hole, which retraces the electron path in the reverse direction (Andreev reflection, Ref. [13]).

There is a fundamental relationship between the 'microscopic' phases of normal quasiparticles reflected from the N/S interface and the macroscopic phase ϕ of the superconducting condensate. A reflected hole acquires an additional phase shift equal to the phase ϕ of the superconductor. Accordingly, reflection turns the hole into an electron whose phase is shifted by $-\phi$.

If the interfering particles are reflected from various superconductors or from various points of the same superconductor, with phases ϕ_1 and ϕ_2, the result of the interference, and hence the quantum conductivity corrections, will depend on the phase difference $\Delta\phi = \phi_1 - \phi_2$. These phase-sensitive materials are of interest not only from a scientific point of view, but also from the practical viewpoint, because they offer the prospect of exploiting phase-controlled conductivity in electron device design.

The following is a brief survey of the work on mesoscopic N/S structures. Emphasis is placed on experimental results because a complete theory of the observed phenomena is still lacking.

Experimental. The maximum size of a mesoscopic structure should not exceed the conduction-electron phase-breaking length $L\phi = (D\tau_\phi)^{1/2}$, where τ_ϕ^{-1} is the sum over the rates of the phase-breaking scattering processes, and D is the electron diffusion constant.

Because the values of $L\phi$ in disordered thin-film samples are in the range 100 – 1000 nm, the fabrication of metallic interferometers with mirrors of different materials requires multilayer lithography with submicron precision for the alignment of different layers. Examples of hybrid mesoscopic structures are shown in Fig. 1. They are normal thin-film structures with controlled-geometry islands with superconducting material deposited on the surface.

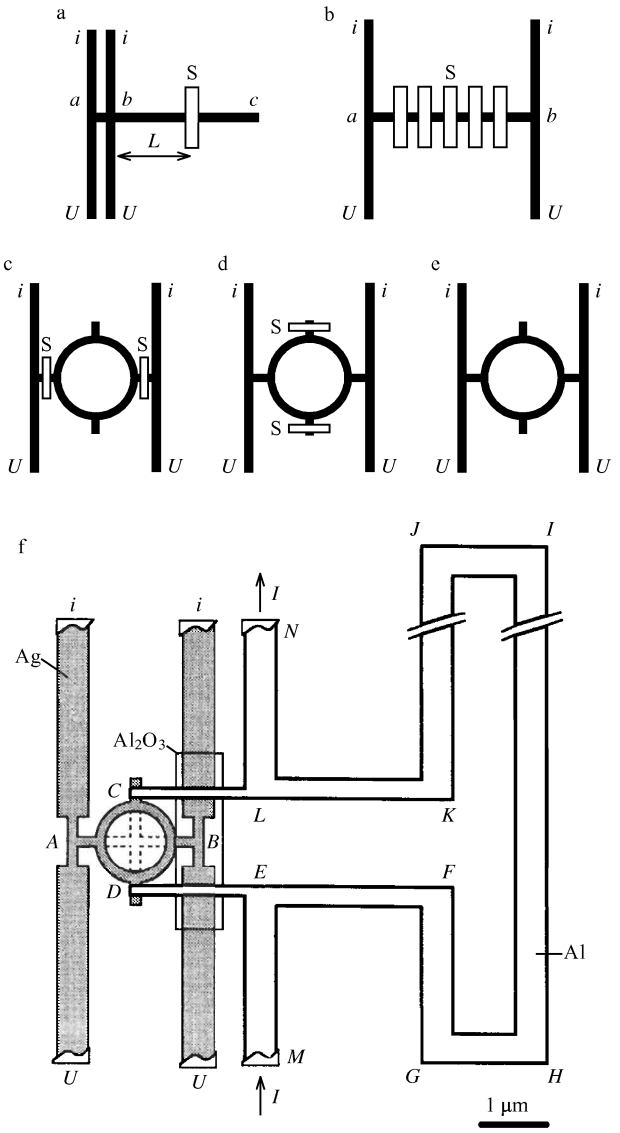

Figure 1. Examples of hybrid mesostructures. Shaded: normal conductors of cross section 100 × 50 nm; unshaded: superconductors; $i-i$ and $U-U$ are the current and potential electrodes, respectively. Rings are 1 μm in diameter.

The normal parts of the structures were disordered silver, bismuth, or nickel films. The transport mean free path in such films was about 10 nm, corresponding to a diffusion constant of $D \approx 10$ cm^2 s^{-1}. The conductors were 100 × 50 nm in cross section. The superconducting materials used were aluminium, tin, lead, and niobium. Measurements were conducted at temperatures of 0.02–4.2 K at frequencies of 30–300 Hz and magnetic fields up to 10 kG.

Anomalous proximity effect and 'dielectrisation' of mesoscopic N/S structures. According to the 'classical' theory (see, for example, [14]), a thin normal-metal layer adjacent to a superconductor must become superconducting as a result of superconducting correlation ('proximity effect'). When a mesoscopic system develops superconducting regions, it has been shown [4] that its normal regions

may transform into states with either increased or reduced conductivity.

The structures studied were made of silver with an H-like part and stubs *bc* 1.2 μm long (Fig. 1a), with aluminium strips S at various distances L from the point *b*. The resistance of the segment *ab*, 0.2–0.3 μm long, was measured with a four-point technique. The measurements were conducted simultaneously on simultaneously fabricated structures sharing the same substrate.

It was found that different structures differed not only in the magnitude of the effect but even in its sign. As the temperature was lowered, some of the samples exhibited a sharp *increase* in the resistance R_{ab} near the transition of the aluminium film to a superconducting state. Such behaviour cannot be explained in terms of the usual proximity effect, which predicts a drop in the resistance of a normal conductor in contact with a superconductor.

As the current or magnetic field was increased, the volt–ampere characteristics and magnetoresistance curves exhibited transitions to lower or higher resistance states. The signs and magnitudes of the effects were the same for the field, current, and temperature.

In addition to the higher resistance transitions, one further surprising result was the strong influence exerted by the superconductor at distances more than an order of magnitude greater than the normal metal coherence length. The change in the conductance $G = 1/R$ (where R is the total resistance) exceeded $\Delta G = \pm 10^3 e^2/h$, indicating the violation of the universality rule, $\Delta G = \pm 1$, in the structures studied.

Further experiments [5] showed that the anomalous long-range proximity effect exists even in ferromagnetic mesoscopic structures and therefore is not connected with the ordinary superconducting correlation, the violation of which occurs in ferromagnetics at about interatomic distances.

A complete theory of the anomalous proximity effect is not available. Numerical calculations [15] suggest the possibility of transitions to higher-resistance states for mesoscopic systems with superconducting islands.

One further structure that was investigated is shown in Fig. 1b. Across a narrow strip of a normal metal, quite closely spaced strips of superconductor S are deposited. When the lead strips became superconducting, the resistance of the segment *ab increased*.

It was found that, in terms of magnetic field values, there exist two regions where the resistance changes are particularly sharp: relatively strong fields close to the critical field B_c for the superconductor, and weak fields $B \ll B_c$. The temperature dependence of magnetoresistance was different in these regions.

For $B \approx B_c$, the total resistance change was practically temperature independent. In weak fields, the resistance change was sensitive to both the temperature and the method of sample preparation. This means that magnetoresistance mechanisms for weak and strong fields are different and may involve different electron groups [11].

'Giant' Aharonov–Bohm oscillations and oscillation frequency doubling. The temperature-dependent magnetoresistance in weak fields may be due to the Andreev-reflection enhanced contribution of weakly localised electrons. Because of reflection, some of the normal electrons are unable to escape to 'infinity' via the current leads and so are localised in the normal region.

The N/S interface then does not prevent the passage of electric current, and this leads to free boundary conditions for the diffusion equation for the quantum interference conductivity correction [16]. What happens is, in a sense, a 'coherent trapping' of conduction electrons in the normal region.

As a consequence, one expects a large increase in the amplitude of Aharonov–Bohm oscillations in the normal rings between superconducting 'mirrors', because the oscillations are of identical nature to the weak-localisation magnetoresistance.

The oscillation enhancement effect was observed experimentally [2] on rings with superconducting strips deposited on current leads (Fig. 1c).

The enhancement of the Aharonov–Bohm effect may also be due to sources unrelated to the trapping of electrons between the mirrors. If the normal regions near superconductors display coherent phenomena similar to those seen in superconductors near the superconducting transition, then oscillations with the same period and a larger-than-normal amplitude can be expected [17].

The contributions of the above mechanisms were determined by experiments [3] on three types of silver rings, the geometry of which is shown in Figs 1c – 1e. In the case (c), the superconducting mirrors were placed on the current leads, as in the experiments of Ref. [2] ('longitudinal' or L mirrors). In (d), they were located at silver stubs (which were set perpendicular to the current lines) at approximately the same distances from the rings as in the (c) case ('transverse' or T mirrors).

While in terms of the usual proximity effects the influence of the superconductors on the ring conductance must be the same in both cases, in the T geometry the electrons were free to leave the rings via the current leads and hence no trapping occurred. For comparison purposes, measurements on rings with no superconducting mirrors were also made (Fig. 1e).

The three structures were found to be quite different in their transport properties. In weak magnetic fields, the amplitude of the magnetoresistance oscillations with a period corresponding to the quantum $\Phi_0 = h/2e$ was enhanced by two orders of magnitude in rings with L mirrors compared to that of rings without mirrors. In the spectrum of T-mirror rings, it was found that, in addition to the enhanced $h/2e$ component, at sufficiently low temperatures an $h/4e$ periodic component existed.

The doubling of the oscillation frequency was qualitatively explained as being due to the effect exerted on weak localisation by the quasiparticles counterpropagating in closed (self-intersecting) diffusion trajectories with Andreev reflections from *different* superconductors. Such trajectories were first considered in Ref. [18]. As the superconductors develop a phase difference $\Delta\phi$ between each other, the counterpropagating electron waves acquire a phase difference of $\delta\phi = 2\Delta\phi$ [18].

In a magnetic field, the total wave phase difference includes the Aharonov–Bohm phase, $2\pi\Phi/\Phi_0$, and the Andreev reflection phase, where also $\Delta\phi = 2\pi\Phi/\Phi_0$ (where Φ is the magnetic flux through the electron trajectory); see Ref. [14]. With the phase shifts added, the oscillation period becomes $\Phi_0/2 = hc/4e$.

In principle, a doubling of oscillation frequency should also be observed in the L geometry, but this requires the adiabaticity condition or, in other words, rules out the

retardation effect: the phase difference change between the superconductors must be small during the time the electron diffuses between them. When the measurement current flows in the L geometry, a potential difference U develops between the superconductors, and, by the Jefferson relation, the phase difference is time dependent, $\Delta\phi(t) = 2eUt/h$.

A sufficiently strong current invalidates the adiabaticity condition, which is why no $h/4e$ period is present. By decreasing the measurement current in the L geometry it is possible to transfer to the adiabatic regime and to observe the $h/4e$ component in the magnetoresistance oscillation spectrum. Such a transition was seen in Ref. [6].

Retardation effects, and, as a consequence, the disappearance of the $h/4e$ component, may also be observed in the T geometry, in which a finite potential difference between the mirrors may result from the fact that the quarter-circle arcs of the rings are in practice different in resistance [7].

The enhancement of the $hc/2e$ oscillation both in the L and T geometries raises the question of whether the 'trapping' of the particles between the mirrors is indeed important. However, when electrons are prevented from leaving the ring via the current leads, it has been shown [18] that the oscillation amplitude increases considerably.

To demonstrate this effect, silver rings with normal bismuth current leads were studied. In this case the ring–lead interface acts as a semitransparent mirror for electrons because of the large difference in the size of the Fermi surfaces of bismuth and silver.

Mesoscopic interferometers with phase control. There are several ways in which the phase difference between T mirrors, and hence the conductivity of a mesoscopic structure, may be controlled.

If T mirrors are connected to different points on a current-carrying superconducting wire, a phase difference must form, proportional to the phase gradient in the superconductor which in its turn is proportional to the supercurrent. Such a system must give rise to periodic resistance oscillations as a function of the supercurrent: a direct result of the transfer of the macroscopic phase from superconducting condensate to normal quasiparticles. This phenomenon was reported in Refs [9, 10].

The geometry of the experiment is shown in Fig. 1f. It is similar to T geometry. The only difference is that the T mirrors of Fig. 1f are connected with an aluminium wire $MEFGHIJKLN$. Comparisons were made with conductivity measurements on a structure with a singly connected cross-shaped conductor instead of a ring (dashed line in Fig. 1f).

Fig. 2 presents the resistance of the segment AB of the normal cross-shaped structure as a function of superconducting current in the aluminium wire at 0.02 K. Note the periodic variation of the normal resistance with supercurrent. Similar oscillations were seen in ring-shaped normal structures connected to a superconductor.

The oscillations can be accounted for by the fact that the contribution of the interfering electrons to the conductivity is changed as the phase of the superconducting condensate is transferred to normal electrons in an Andreev reflection. In the absence of a magnetic field, passing a supercurrent I gives rise to a phase shift, between the electrons reflected from the N/S interfaces at C and D, amounting to

$$\Delta\varphi_{CD} = 2\pi \frac{L_{\text{eff}}}{\Phi_0} I \,.$$

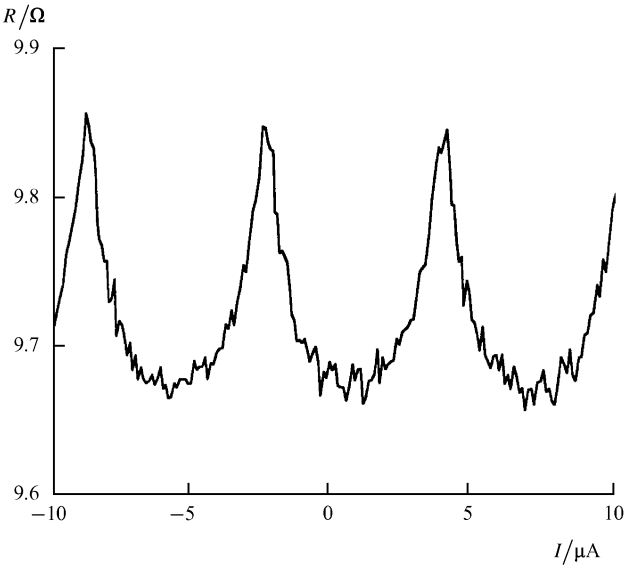

Figure 2. Resistance of the segment AB of the normal (silver) part of the cross-shaped structure (Fig. 1f) versus superconducting current through the aluminium wire $MEFGHIJKLN$ at $T = 0.02$ K [10].

Here L_{eff} is the effective inductance of the superconducting wire segment between points E and L.

Oscillations are also observed in a magnetic field perpendicular to the substrate. An example for a normal ring-shaped structure is illustrated in Fig. 3. The high oscillation frequency corresponds to the penetration of the flux quantum Φ_0 through the area bounded by the middle line of the superconducting loop. The upper and lower envelopes are due to the penetration of quantum fluxes $\Phi_0/2$ and Φ_0 through the normal ring.

Although the origin of the oscillations may be considered established, their detailed mechanism is not yet understood. No satisfactory explanation has been given for the line shape, nor for the period and phase of the oscillations, or the pattern of oscillation in a magnetic field (Fig. 3). A quantitative theory would turn the above measurements into a unique and powerful investigation tool.

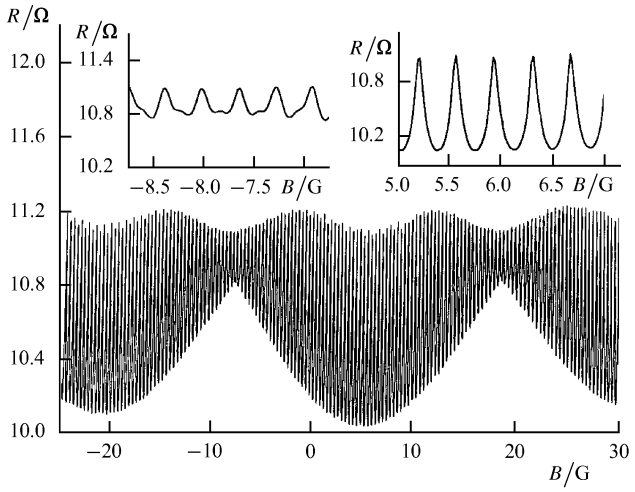

Figure 3. Resistance of the segment AB of the normal part of the ring structure (Fig. 1f) versus magnetic field normal to the substrate, at $T = 0.02$ K [10].

References

1. Petrashov V T, Antonov V N *Pis'ma Zh. Exp. Teor. Fiz.* **54** 245 (1991) [*JETP Lett.* **54** 241 (1991)]
2. Petrashov V T, Antonov V N, Persson M *Physica Scripta* **42** 136 (1992)
3. Petrashov V T, Antonov V N, Delsing P, Claeson T *Phys. Rev. Lett.* **70** 347 (1993)
4. Petrashov V T, Antonov V N, Maksimov S V, Shaikhaidarov R Sh *Pis'ma Zh. Exp. Teor. Fiz.* **58** 48 (1993) [*JETP Lett.* **58** 49 (1993)]
5. Petrashov V T, Antonov V N, Maksimov S V, Shaikhaidarov R Sh *Pis'ma Zh. Exp. Teor. Fiz.* **59** 523 (1994) [*JETP Lett.* **59** 551 (1994)]
6. Antonov V N, Cand. Diss. Thesis (Chernogolovka: IPTM RAN, 1994)
7. Petrashov V T, Antonov V N, Delsing P, Claeson T *Physica B* **194–196** 1105 (1994)
8. Petrashov V T, Antonov V N, Maksimov S, Shaikhaidarov R, in *Int. Conf. on the Physics and Technology of Metallic Nanostructures: Metallic Nano-Electronics, Chernogolovka, 12–15 September 1994*
9. Petrashov V T, Antonov V N, Delsing P, Claeson T, submitted to *Phys. Rev. Lett.* (1994)
10. Petrashov V T, Antonov V N, Delsing P, Claeson T *Pis'ma Zh. Eksp. Teor. Fiz.* **60** 589 (1994) [*JETP Lett.* **60** 606 (1994)]
11. Petrashov V T *Mikroelektronika* **23** 3 (1994) [*Russ. Microelectron.* **23** 261 (1994)]
12. de Vegvar P G N, Fulton T A, Mallison W H, Miller R E *Phys. Rev. Lett.* **73** 1416 (1994)
13. Andreev A F *Zh. Exp. Teor. Fiz.* **46** 1823 (1964) [*Sov. Phys. JETP* **19** 1228 (1964)]
14. Abrikosov A A *Osnovy Teorii Metallov* (Principles of the Theory of Metals) (Moscow: Nauka, 1987)
15. Hui V C, Lambert C J *Europhys. Lett.* **23** 203 (1993); Lambert C J, Robinson S J *Physica B* **194–196** 1641 (1994)
16. Al'tshuler B L, Aronov A G, Zyuzin A Yu *Zh. Exp. Teor. Fiz.* **86** 709 (1984) [*Sov. Phys. JETP* **59** 415 (1984)]
17. Larkin A I *Pis'ma Zh. Exp. Teor. Fiz.* **31** 239 (1980) [*JETP Lett.* **31** 219 (1980)]
18. Spivak B Z, Khmel'nitskii D E *Pis'ma Zh. Exp. Teor. Fiz.* **35** 334 (1982) [*JETP Lett.* **35** 412 (1982)]

PACS numbers: 61.60.Ch

Effects of localised states and interparticle interactions on the STM/STS and AFM nanostructure diagnostics

N S Maslova, Yu N Moiseev, V I Panov, S V Savinov

The advent of scanning tunnelling microscopy (STM) provided a number of novel methods both for nanostructure diagnostics and for investigating physical processes taking place on solid surfaces and interfaces. These methods have recently been given the generic name 'nanoscopy' and include STM/STS, atomic force microscopy (AFM), optical near-field microscopy, and capacitor and magnetic strength microscopy.

However, only STM/STS and AFM permit atomic spatial resolution and enable a wide variety of properties and processes to be investigated in nanostructures, and it is primarily these methods which are being used to modify the topological and electronic properties of the near-surface layers of solid-state and molecular structures.

However, in spite of the numerous experiments carried out with these methods, many questions remain as to the effect that individual localised states and interparticle interactions have on tunnelling processes in nanometer-sized contacts and on the STM/STS and AFM data.

For this reason, we will be mainly concerned with experimental and theoretical results which involve the influence of localised states and of interparticle interactions on tunnelling and which enable adequate description of STM/STS and AFM experiments.

The influence of localised states on tunnelling processes in nanostructures and low-dimensional systems is significant for the following reasons:

(1) reducing the tunnelling barrier width to an interatomic scale causes a significant rearrangement of the initial electron spectrum owing to hybridisation effects;

(2) when a characteristic localisation length and the size of the tunnel junction are of the same order, the nature of tunnelling may be determined by the properties of a localised state;

(3) in low dimensions, the energy levels of bound localised states may shift into the gap even if the initial impurity levels are below the valence band edge;

(4) the finite relaxation time of nonequilibrium electrons considerably changes the time characteristics of the tunnel current, particularly when localised states are present.

Experimental studies were made in which the STM/STS and AFM methods were used. In nanometer-sized tunnelling structures formed by the STM point and the surfaces of various ordered monomolecular layers, periodic charge density wave (CDW) structures, both commensurate and incommensurate with the molecular lattice periods, were seen (Fig. 1).

The CDW periodic structures can be seen in an STM image at energy $eV_t \ll \Delta$ (where Δ is the CDW energy gap, $\Delta > kT$). This indicates that bound localised levels associated with tunnelling channels exist in the gap.

Because of the hybridisation effects, such in-gap levels (i) cause an abrupt (two to three orders of magnitude) tunnelling conductivity increase as the STM point–surface distance is reduced by $\Delta z \approx 0.1$ nm; (ii) give rise to negative

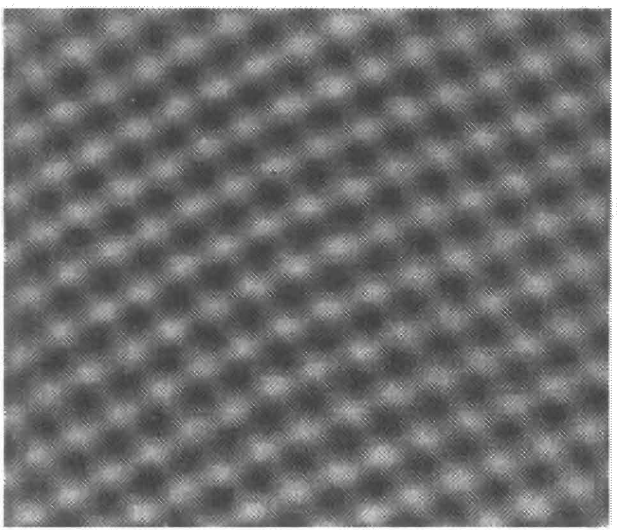

Figure 1. STS image of the volt–ampere characteristic at the surface of a monomolecular Langmuir film.

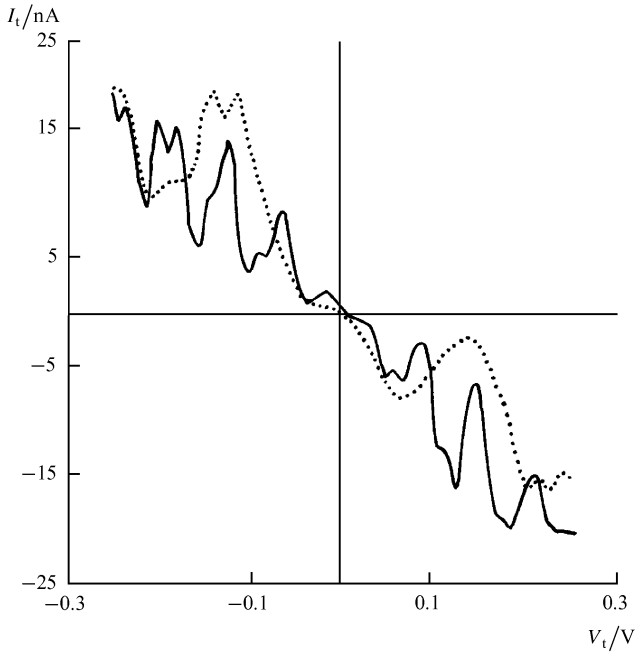

Figure 2. Volt–ampere characteristic of a tunnelling junction above various portions of a monomolecular Langmuir film.

conductivity portions in the tunnelling volt–ampere characteristic $I_t(V_t)$ (Fig. 2); and (iii) produce oscillations in the tunnelling current I_t as a function of the interelectrode spacing Δz (Fig. 3).

It should be noted that density-of-states oscillations and sharp tunnelling conductivity increases occur in tunnelling contacts formed by cluster systems and an STM point. However, these kinds of effect are particularly pronounced if there are defects and impurities present on the electrode surfaces; presumably evidence for the existence of localised levels within them.

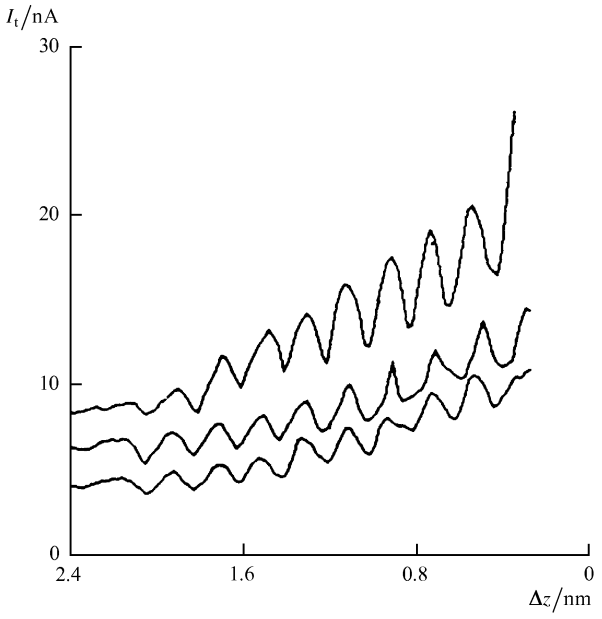

Figure 3. Oscillations in the tunnelling current against the distance between the STM point and the surface of the molecular film for various tunnelling voltages.

The appearance of localised states on a semiconductor surface may drastically alter the time characteristics of the tunnelling current.

The STM/STS images of the surface of boron-doped silicon were found to display regions, about 2 nm in size, in which volt–ampere characteristics, $I_t(V_t)$, displayed 1.2 eV features. Increasing the scanning speed decreases the contrast of those surface regions formed by the tunnelling current intensity. Moreover, such regions become virtually invisible for measurements at potential difference V_t less than the peak value on $I_t(V_t)$.

In our view, the surface regions showing features in the $I_t(V_t)$ or $\partial I/\partial V$ plots provide evidence that individual states have localisation radius greater than both the tunnel junction size and the barrier width. As a result, the tunnelling current may to a large extent be governed by the energy characteristics of these states, provided the junction potential difference is equal to or greater than their energy.

Under these conditions there is a contribution to the tunnelling current from fluctuations typical of a telegraph-noise spectrum with several discrete amplitudes and periods. The implication is that nonequilibrium electronic processes contribute to tunnelling within the localisation regions.

The results obtained were explained in terms of the self-consistent theory of tunnelling, which takes into account the electronic spectrum renormalisation, the finite relaxation time of the nonequilibrium electrons, and Coulomb correlations. Within this model we were able (i) to obtain a general expression for the tunnelling current through bound localised states, taking account of the nonmonotonic nature of the tunnelling junction volt–ampere characteristic, and (ii) to evaluate the energies of the bound localised gap states which, for the quasi-one-dimensional and quasi-two-dimensional electronic density-of-states functions at the edge of the sample spectrum are, respectively,

$$\tilde{E}_d = E_v + \frac{1}{W_1}\left(\frac{V^2}{E_v - E_d}\right)^2 ,$$

$$\tilde{E}_d = E_v + W_2 \exp\left(-W_2 \frac{\tilde{E}_d - E_d}{V^2}\right) ,$$

where E_v is the valence band edge, V the tunnelling amplitude, and W_1 and W_2 are typical band widths. It follows from this that the position of the levels involved depend on the junction voltage and the interelectrode separation.

Of major concern in the present study was the effect of the intra-site Coulomb repulsion of the position of the level. The localisation radius of the states is estimated to be

$$R_0 \approx a\left(\frac{W}{\tilde{E}_d - E_v}\right)^{1/D} ,$$

where D is the structure dimensionality and a its period.

Attention is also given to the nonstationary tunnelling from localised states in the presence of Coulomb correlations. The time dependence of the tunnelling current is derived and its relative fluctuations are estimated.

The results above suggest that as the size of the nanostructure is reduced, localised states may dominate tunnelling processes, introducing substantial changes in the electronic properties of the structure.

At the same time, individual localised states that form resonant tunnelling channels may, within the localisation radius, be identified with a nanometer-sized tunnelling structure. However, there are as yet unanswered questions concerning the fabrication of such structures with reliably reproducible and controlled parameters.

The results presented in the final portion of the talk illustrated the use of nanoscopy in physical studies and precision measurements. These include the observation of the surface diffusion of single atoms and small metallic clusters; the elucidation of the nature of giant reflection under nonlinear-optics conditions from a nonuniform metal surface; the study of the photoconductivity of single organic molecules; the determination of the topology of carbon nanopipe molecules; interface diagnostics; the use of STM for single-molecule manipulation, for surface modification, and in short-replacement transducer design; the use of AFM in interatomic interaction spectroscopy, in experiments on the determination of the parameters of hypothetical long-range forces, etc.

The work has been supported in part by the "Solid Nanostructure Physics" Program (No. 1-032), the RFRF Project (No. 93-02-2214), and the ISF Project (No. M5D000).

References

1. Aksipetrov O A, Nikulin A A, Panov V I, Vasil'ev S I *Solid State Commun.* **73** 411 (1990)
2. Maslova N S, Moiseev Yu N, Panov V I, et al. *Phys. Stat. Sol. A* **131** 35 (1991)
3. Maslova N S, Moiseev Yu N, Panov V I, et al. *Zh. Exp. Teor. Fiz.* **102** 925 (1992) [*Sov. Phys. JETP* **75** 505 (1992)]
4. Arseev P I, Maslova N S, *Zh. Exp. Teor. Fiz.* **102** 1056 (1992) [*Sov. Phys. JETP* **75** 528 (1992)]
5. Maslova N S, Moiseev Yu N, Savinov S V, Yusupov P G *Pis'ma Zh. Exp. Teor. Fiz.* **58** 524 (1993) [*JETP Lett.* (1993)]
6. Chernozatonskii L A, Fedorov E A. Kosakovskaya Z Ya, et al. *Pis'ma Zh. Exp. Teor. Fiz.* **57** 35 (1993) [*JETP Lett.* **57** 35 (1993)]
7. Todorov T N, Briggs G A D, Sutton A P *J. Phys. Cond. Matter* **5** 2389 (1993)
8. Moiseev Yu N, Panov V I, Savinov S V, Yaminsky I V *J. Vac. Sci. Technol. B* **12** 1690 (1994)